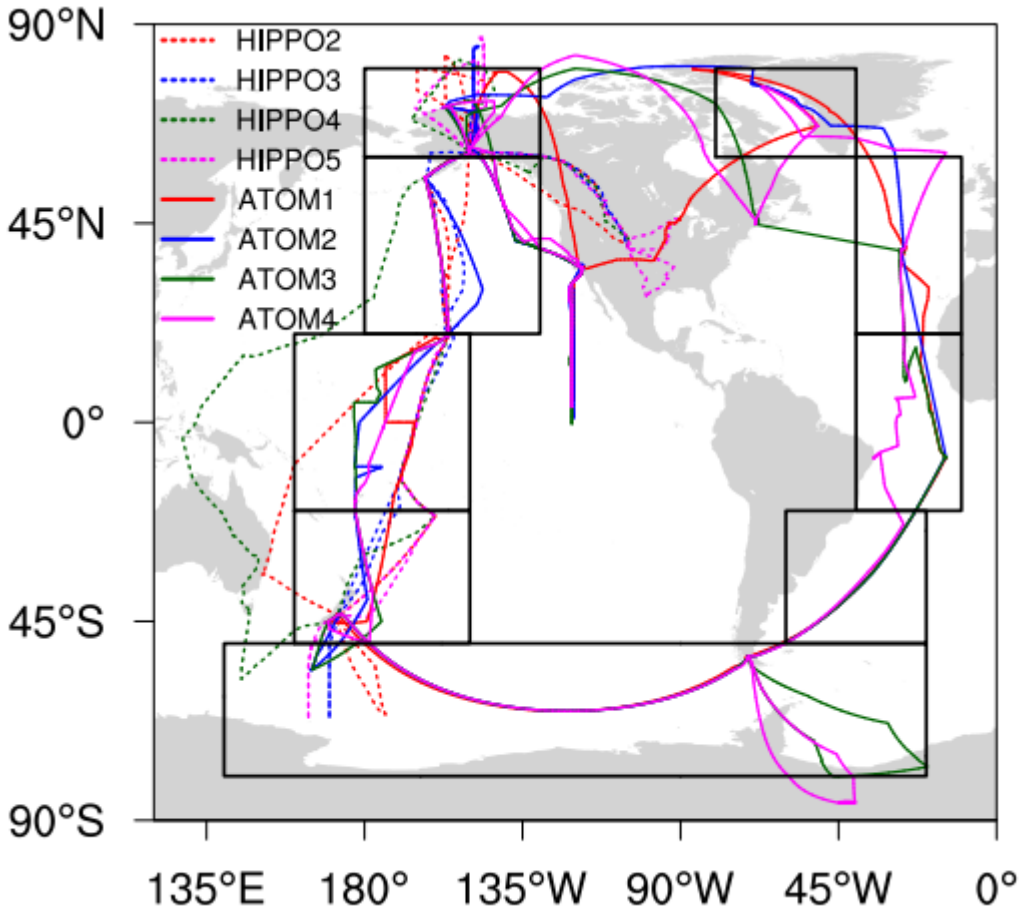

Fig. S1. Flight routes from eight deployments of HIPPO and ATOM campaigns. The observations are divided into nine latitude bands (shown in black boxes) for comparison with model results.

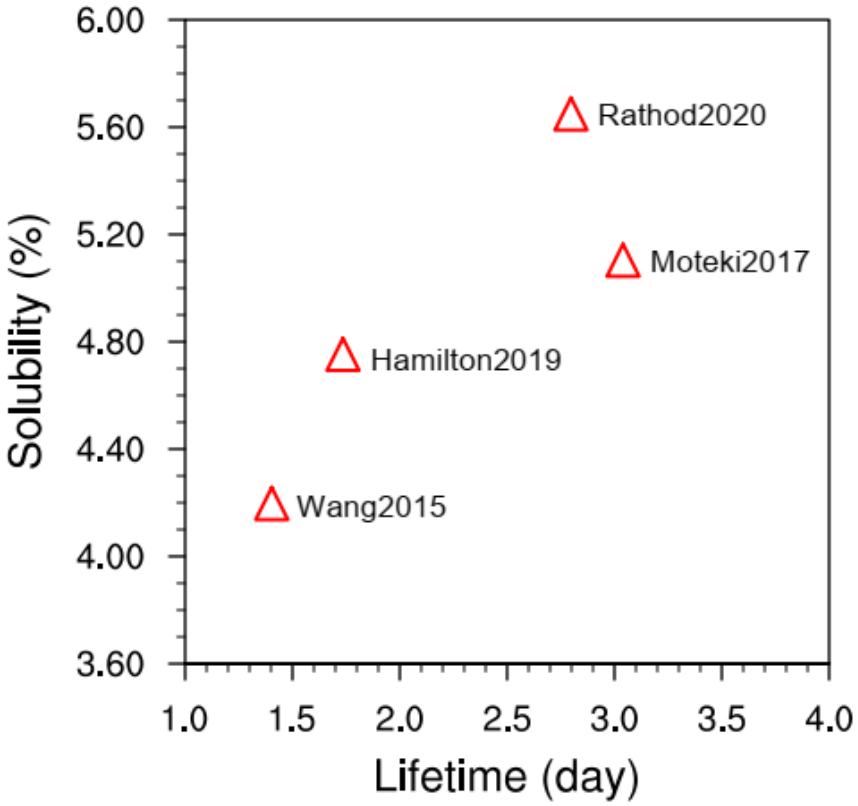

Fig. S2. Ratios of anthropogenic and total iron deposition in the fine-sized case to those of coarse-sized case.

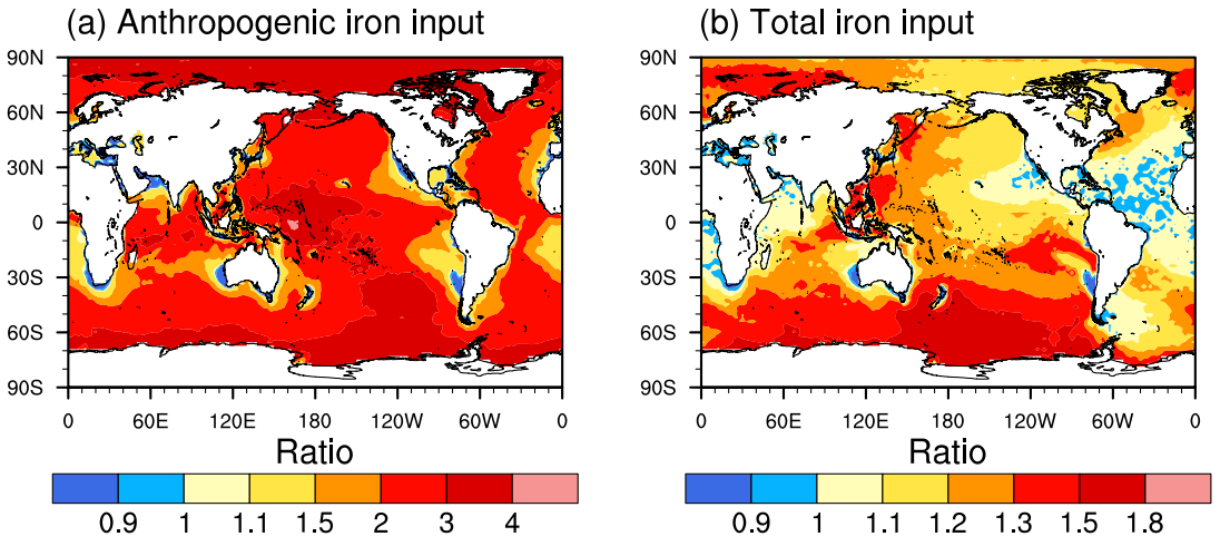

Fig. S3. Ratios of anthropogenic and total iron deposition in the fine-sized case to those of coarse-sized case.

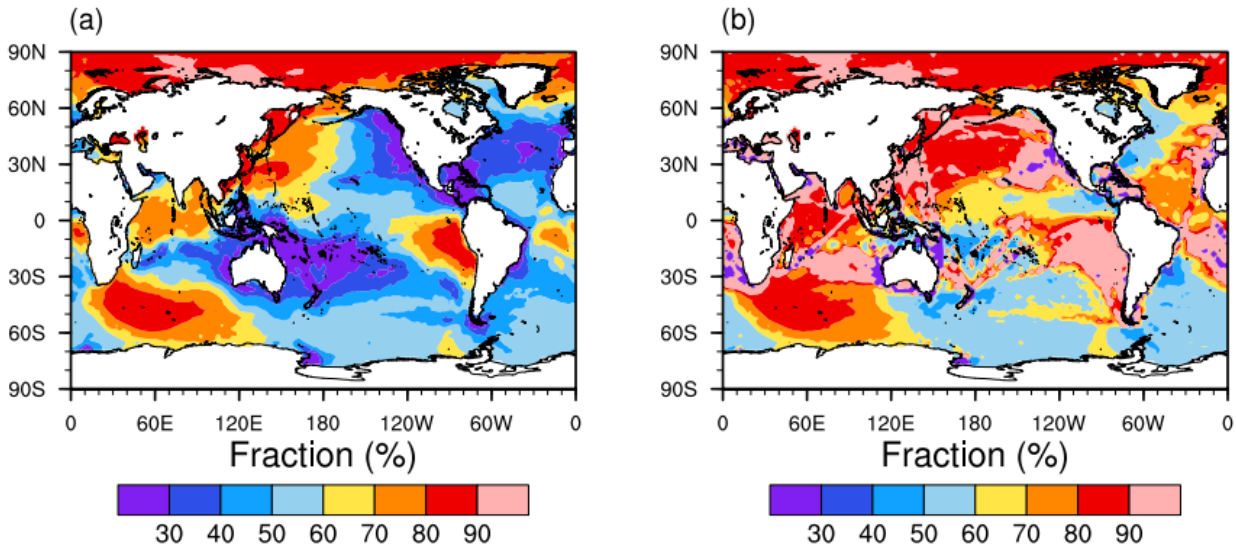

Fig. S4. Fractional contributions of aerosol aging processes to soluble iron deposition in the fine-sized case (a) and to the differences between the fine-sized and coarse-sized cases (b). The fractions are derived by comparing the differences between the cases with and without aerosol aging processes for both the fine-sized and coarse-sized cases.

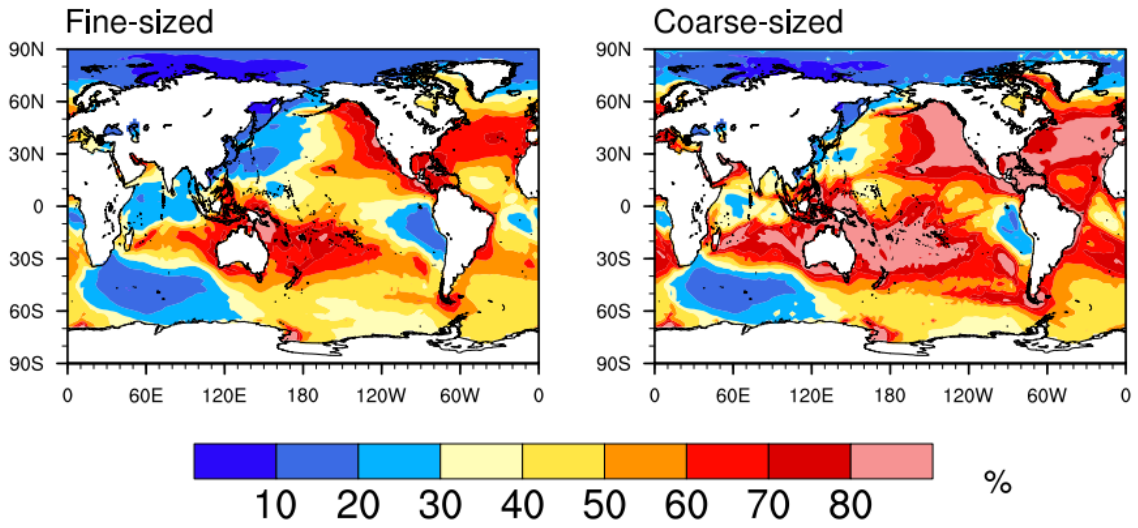

Fig. S5. Contribution of iron sulfates to total soluble iron deposition originating from anthropogenic sources. Here, results of the simulations with the fine-sized and coarse-sized iron emissions are shown for comparison.

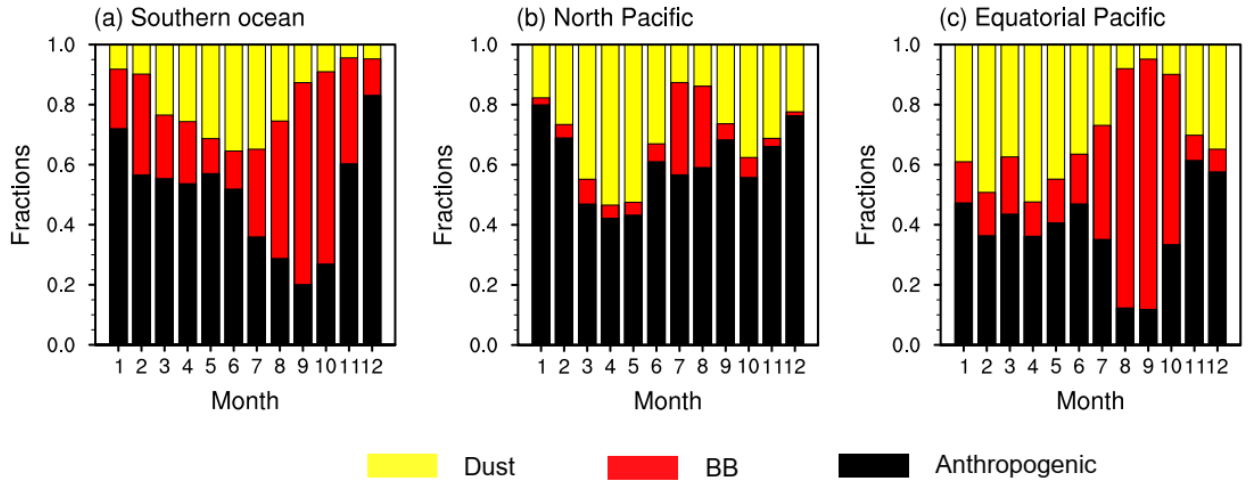

Fig. S6. Source appointments of monthly soluble iron deposition over three ocean basins. The results are the averages of all simulation years (2009-2011 and 2016-2018).